Characterizing the Effects of Synergistic Thermal and Photocrosslinking during Biofabrication on the Structural and Functional Properties of Gelatin Methacryloyl (GelMA) Hydrogels

Parth Chansoria, PhD ^{1,2, \delta}, Suleman Asif ^{1,2}, Kathryn Polkoff ^{2,3}, Jaewook Chung, PhD ^{2,3}, Jorge A. Piedrahita, PhD ^{2,3}, Rohan A. Shirwaiker, PhD^{1,2,4,5}*

AUTHOR ADDRESS

- Edward P. Fitts Department of Industrial and Systems Engineering, North Carolina State University, Raleigh, NC 27695, USA
- ² Comparative Medicine Institute, North Carolina State University, Raleigh, NC 27606, USA
- Department of Molecular Biomedical Sciences, North Carolina State University, Raleigh, NC 27606, USA
- Joint Department of Biomedical Engineering, University of North Carolina at Chapel Hill and North Carolina State University, Raleigh, NC 27695, USA
- Department of Mechanical and Aerospace Engineering, North Carolina State University, Raleigh, NC 27695, USA
- * Corresponding author. Email: rashirwaiker@ncsu.edu

ABSTRACT

Gelatin methacryloyl (GelMA) hydrogels have emerged as promising and versatile biomaterial matrices with applications spanning drug delivery, disease modeling, and tissue engineering and regenerative medicine. GelMA exhibits reversible thermal crosslinking at temperatures below 37°C due to the entanglement of constitutive polymeric chains, and subsequent ultraviolet (UV) photo-crosslinking can covalently bind neighboring chains to create irreversibly crosslinked hydrogels. However, how these crosslinking modalities interact and can be modulated during biofabrication to control the structural and functional characteristics of this versatile biomaterial is not well explored yet. Accordingly, this work characterizes the effects of synergistic thermal and photo-crosslinking as a function of GelMA solution temperature and UV photo-crosslinking duration during biofabrication on the hydrogels' stiffness, microstructure, proteolytic degradation, and responses of NIH 3T3 and human adipose-derived stem cells (hASC). Smaller pore size, lower degradation rate, and increased stiffness are reported in hydrogels processed at lower temperature or prolonged UV exposure. In hydrogels with low stiffness, the cells were found to shear the matrix and cluster into micro-spheroids, while poor cell attachment was noted in high stiffness hydrogels. In hydrogels with moderate stiffness, ones processed at lower temperature demonstrated better shape fidelity and cell proliferation over time. Analysis of gene expression of hASC encapsulated within the hydrogels showed that while the GelMA matrix assisted in maintenance of stem cell phenotype (CD44), a higher matrix stiffness resulted in higher pro-inflammatory marker (ICAM1) and markers for cell-matrix interaction (ITGA1 and ITGA10). Analysis of constructs with ultrasonically patterned hASC showed that hydrogels processed at higher temperature possessed lower structural fidelity but resulted in more cell elongation and greater anisotropy over time. These findings demonstrate the significant impact of GelMA material formulation and processing conditions on the structural and functional properties of the hydrogels. The understanding of these material-process-structure-function interactions is critical towards the optimizing the functional properties of GelMA hydrogels for different targeted applications.

Keywords: GelMA, Thermo-reversible crosslinking, Photo-crosslinking, Biofabrication, Tissue engineering, CryoSEM, qPCR

1. Introduction

Gelatin methacryloyl (GelMA) hydrogels have garnered significant interest toward a variety of biomedical applications owing to their highly desirable biochemical and biophysical characteristics of GelMA solution are similar to those of pure gelatin. These include similarity in rheological properties such as swelling and shear thinning, thermo-reversible crosslinking at lower temperatures, and the presence of arginine-glycine-aspartic acid (RGD) and matrix metalloproteinase (MMP)-cleavable sequences that provide an ideal environment for cells to attach and proliferate to form a tissue¹. Methacrylation of the lysine groups in the gelatin backbone renders photo-crosslinkability to GelMA². In the presence of a photoinitiator within the solution, the methacrylate moieties within and between neighboring polymeric chains can be covalently bound upon UV exposure^{2,3}, leading to an irreversibly photocrosslinked matrix. This stable matrix and its biocompatible and biodegradable properties offer a wide variety of applications such as scaffolds for tissue engineering¹ and drug delivery^{4,5}, wound healing⁶, biological templates for studying disease progression⁷, and extrusion² and VAT photopolymerization bioprinting⁸.

Figure 1(a) illustrates the crosslinking mechanisms of GelMA hydrogels. The processing conditions during biofabrication govern these mechanisms, ultimately affecting the structural, mechanical and biological characteristics of the crosslinked hydrogel. As such, reducing the temperature of GelMA solution below the typical physiological temperature (37°C) induces thermo-reversible crosslinking through entanglement of neighboring polypeptide chains into networks^{1,9}. Herein, GelMA is able to de-crosslink and return back to a liquid state once the temperature is increased (hence the thermo-reversibility)¹. Interestingly, once the GelMA is in a thermally crosslinked state, inducing photo-crosslinking of the GelMA in the presence of a photoinitiator leads to covalent bonding between the neighboring methacrylate groups, entrapping the polypeptide chains in their entangled state and leading to an irreversible crosslinking.

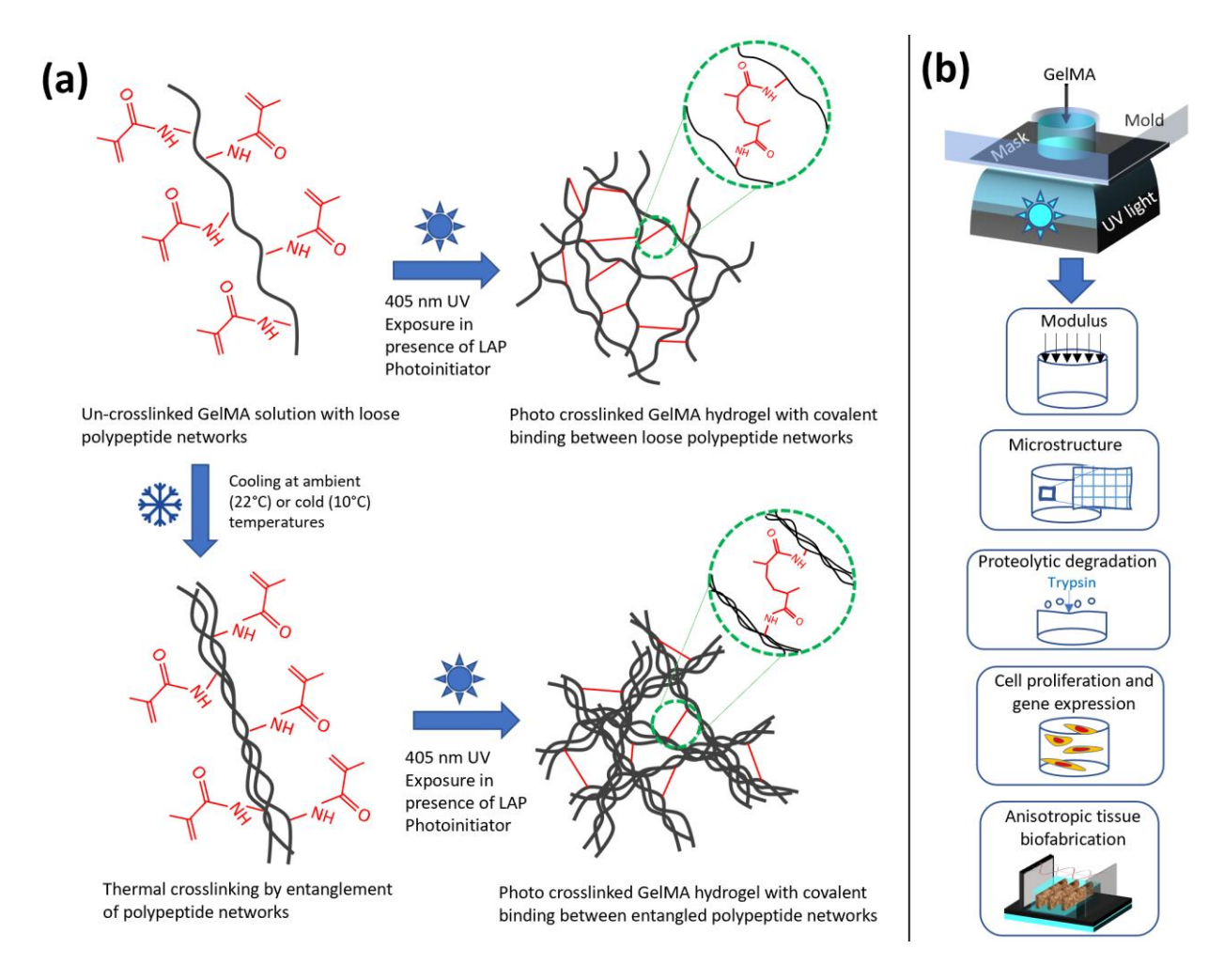


Figure 1. (a) Creating photo-crosslinked GelMA constructs with or without thermally-induced crosslinking, and **(b)** the constitutive studies in this work.

One approach to alter the properties of the hydrogel to suit various applications is to modify the material composition (e.g., degree of substitution and concentration, type and concentration of photoinitiator). This approach, including the impacts of independent thermally-induced crosslinking and photo-crosslinking on properties of different compositions of GelMA, has been well studied in literature^{2,10–15}. A complementary, yet under-explored, strategy is to regulate the processing conditions and utilize the synergy between the two crosslinking mechanisms during biofabrication to achieve a broad range of hydrogel functional properties for a given GelMA

composition. With this strategy, the process parameters and resulting crosslinking modalities can be optimized not only to fine-tune the bulk hydrogel properties for a given application, but also to potentially control the properties of the material across space and time during the biofabrication process. Especially given the current trends in the development of new additive and hybrid biofabrication processes and platforms¹⁶, further exploring this process-driven strategy that can enable the regulation of properties of a single material between layers or between successive processing steps would be highly beneficial.

This study investigates the synergy between thermally-induced crosslinking and photocrosslinking in response to the biofabrication processing conditions, and the resulting impact on the functional characteristics of the hydrogels. The effects of two critical process parameters – temperature of GelMA solution prior to photo-crosslinking and ultraviolet (UV) exposure duration during subsequent photo-crosslinking – on the matrix microstructure, 3D cell-matrix interactions, and resultant hydrogel construct functionality and fidelity over time are characterized. Understanding these material-process-structure-function interactions is essential to be able to utilize the fullest potential of hydrogel systems that undergo both thermal and photo-crosslinking. These interactions can be leveraged in future to optimize the hydrogels' structural, mechanical, and biological functional characteristics relevant to its given applications.

2. Materials and methods

The constitutive studies in this work are highlighted in **Figure 1(b)**. First, the stiffness in compression of different compositions of GelMA hydrogels formulated under different thermal and photo-crosslinking conditions were investigated. The GelMA composition that resulted in the broadest range of compressive stiffness relevant for tissue engineering applications was made the

focus of rest of the studies. Scanning electron cryomicroscopy (CryoSEM) was performed to elucidate fundamental changes to the microstructure of GelMA hydrogels under different crosslinking conditions and its relationship with the hydrogel stiffness. The effects of microstructure on the enzymatic degradation of hydrogels were also evaluated. Next, the effects of GelMA microstructure and stiffness on the viability and proliferation of two cell types commonly used in biofabrication – NIH 3T3 cells^{17–19} and human adipose stem cells (hASC)^{20,21} – were investigated. Further, select GelMA hydrogel groups with encapsulated hASC were assessed for their effects on the expression of various genes pertaining to the maintenance of stem cell phenotype²², and cell-cell²³ and cell-matrix interactions^{24,25}. The final study assessed the impact of varying degrees of thermal and photo-crosslinking on the behavior of hASC patterned anisotropically within the GelMA matrices via ultrasound-assisted biofabrication (UAB)^{8,26,27}.

2.1 GelMA solution formulation

The GelMA solution was prepared at a concentration of 5% or 10% w/v by adding the appropriate volume of sterile Dulbecco's phosphate buffered saline (DPBS without phenol red, 25-508B, Genesee Scientific, San Diego, CA) to sterile, lyophilized, porcine-derived (Type A) GelMA with 80% degree of substitution (DOS) or 40% DOS (MilliporeSigma, Burlington, MA). The consistency of the materials was confirmed via ¹H NMR analyses (n = 3 per DOS) (see supporting information Figure S1). The solution was vortexed and allowed to homogenize at 37°C for 1 h. A LAP (Lithium phenyl-2,4,6-trimethylbenzoylphosphinate) photoinitiator (MilliporeSigma) was then added at 0.25% w/v concentration, which is consistent with previous work on GelMA hydrogels^{8,11}. LAP, which has a photoinitiation wavelength of 405 nm²⁸, has been demonstrated

to be more biocompatible during short and long-term culture studies compared to photoinitiators such as the Irgacure 2959^{28,29}, which has a lower photoinitiation wavelength (365 nm).

2.2 Fabrication of GelMA hydrogel constructs

For the compression testing, microstructural analysis, and proteolytic degradation studies, cylindrical GelMA hydrogel constructs ($\emptyset = 7.5$ mm, thickness = 5 mm) were fabricated via casting in negative molds made of a flexible resin (Smooth Cast® 300, Smooth-On Inc., Macungie, PA). In an untreated petri dish (60 mm, Millipore Sigma), 250 µl of GelMA solution at 37°C was added to the mold cavity and thermally or/and photo-crosslinked at different combinations of prephoto-crosslinking solution temperature (37°C, 22°C, 10°C; henceforth referred to as "warm", "ambient", and "cold" hydrogel groups, respectively) and UV exposure duration during subsequent photo-crosslinking (4 s, 6 s, 8 s, 10 s) via a 405 nm UV lamp (Fungdo, Shenzhen Fundo Smart Technology Co. Ltd., China). A distance of 20 mm was maintained between the lamp and the solution during all studies. The radiation intensity at the solution interface was determined using a pyranometer (Tenmars, Taiwan) to be 10 mW/cm². For the warm group, the GelMA solution that was introduced into the mold cavity at 37°C was immediately photo-crosslinked for the appropriate duration. For the ambient and cold groups, the solution was allowed to thermally crosslink for 10 min at 22°C (controlled room temperature) and 10°C (cold water bath), respectively, prior to photo-crosslinking. This duration of thermal crosslinking (10 min) was determined from a supporting study that characterized the compression modulus of hydrogels under different thermal- and photo-crosslinking conditions (see supporting information Figure S2). After photo-crosslinking, the mold was carefully removed from around the discs, and the petri

dishes with the hydrogel discs were incubated at 37°C for 1 h to allow stress relaxation before commencing any testing.

2.3 Determination of compression modulus of hydrogels

To determine the impact of synergistic thermal and photo-crosslinking on the hydrogel stiffness, the constructs made using different GelMA compositions and processing conditions (**Table 1**) were assessed via uniaxial compression testing based on previously established protocols ³⁰. Briefly, after stress-relaxation for 1 h at 37°C, the constructs (n = 3 per group) were subjected to compression in a universal testing system (5 N load cell, Instron, Norwood, MA) with a preload of 0.01 N and a constant strain rate at 0.125 mm/mm/min. The moduli were calculated as the slopes of the resulting stress-strain curves between 0-20% strain.

Table 1. Summary of GelMA hydrogel formulations tested in uniaxial compression

GelMA composition	80% degree of substitution – 5% w/v concentration (80% DOS – 5% w/v) 40% degree of substitution – 5% w/v concentration (40% DOS – 5% w/v) 40% degree of substitution – 10% w/v concentration (40% DOS – 10% w/v)	
Pre-photo-crosslinking solution temperature	Warm (37°C), Ambient (22°C), Cold (10°C)	
UV exposure duration	4, 6, 8, 10 s	

2.4 Evaluation of hydrogel microstructure via CryoSEM

To study the effects of processing conditions on microstructure of GelMA hydrogels, the 80% DOS – 5% w/v composition was selected because it provided the widest range of stiffnesses (as per results in section 3.1). Constructs were fabricated at select combinations of pre-photocrosslinking solution temperature (cold, ambient, warm) and UV exposure duration (0 s (i.e., no exposure), 6 s, 10 s) and analyzed via cryoSEM imaging (n = 3 per group). For imaging, the

cryogenic scanning electron microscope (7600F, ALTO, Gatan, JEOL Ltd, Tokyo, JP) was prepped by adding liquid nitrogen to the sample preparation chamber and SEM stage (and their anticontaminators) to reduce their temperatures to at least -140°C and -165°C, respectively. Using an external vacuum pump, the cryoSEM was maintained at 4×10⁻⁶ mbar during the experiments. All imaging samples, except for the warm-0 s group, were made by slicing the stress-relaxed GelMA constructs into cuboids (60×2×2 mm³) that were then loaded onto the sample holding jigs. As the warm-0 s samples were in a liquid state, 50 μl of the formulation was added to the sample holding cavity within the jigs. The samples on the jigs were then rapidly frozen in slush nitrogen, followed by freeze fracturing inside the preparation chamber. The preparation chamber was heated until -90°C, and the samples were allowed to undergo sublimation for 5 min. The samples were then sputter coated in the presence of Argon at 10 mA for 4 min and transferred to the imaging chamber for viewing and imaging at 1 kV.

The pore sizes within the cryoSEM images were characterized via a custom algorithm developed in MATLAB (**Figure S3 (a)**). Briefly, the scale of the image (3500X) was calibrated as per user input, followed by image binarization and cleaning based on user inputs. The two-dimensional porosity was calculated as per **Equation 1**^{31,32}.

% Porosity =
$$100(1 - \frac{A_{white}}{A_{total}})$$
 (1)

where A_{white} is the area corresponding to the GelMA polymers in the binary image and A_{total} is the total area of the image. Then, each pore was individually identified in the image and the pore size determined as equivalent circle diameter as per **Equation 2**^{31,32}.

Pore size =
$$\sqrt{\left(\frac{4A_{pore}}{\pi}\right)}$$
 (2)

where $A_{pore} = \pi r^2$ is the area of the pore and r is the approximate pore radius. In each image, twenty largest pore sizes were averaged to determine the mean pore diameter for that image. With a sample size of n = 3 per group, mean pore size comprised of an average of 60 pores. Prior to analyzing the cryoSEM images, the accuracy of the algorithm was verified to be 95% by applying it to three images (honeycomb structure, square, and round holes) with known porosities and pores sizes (**Figure S3(b)**).

2.5 Evaluation of proteolytic degradation of hydrogels via trypsin-EDTA

GelMA (80% DOS – 5% w/v) constructs were fabricated at different combinations of pre-photocrosslinking solution temperature (warm, ambient, cold) and UV photo-crosslinking duration (6 s, 10 s) (n = 3 per group). The constructs were weighed and transferred to an untreated petri dish (35 mm, Millipore Sigma). Then, 5 ml of 0.25% trypsin with 0.03% ethylenediaminetetraacetic acid (EDTA, Millipore Sigma) was added and the samples maintained under ambient conditions (22°C) for 30 min. At every 10 min interval, the sample was retrieved from trypsin-EDTA solution, dabbed carefully with a blotting paper, similar to a previous study, 9 and weighed.

2.6 Cell culture and GelMA bioink preparation

The 3T3 fibroblasts (CRL-1658TM, ATCC, Manassas, VA) were cultured (37°C, 5% CO₂) in 90% v/v minimum essential medium without L-glutamine (MilliporeSigma) supplemented with 10% v/v fetal bovine serum (Thermo Fisher Scientific, Waltham, MA). The human adipose-derived

stem cells (hASC, R7788115, ThermoFisher Scientific) were cultured (37°C, 5% CO₂) in MesenPro RS basal media with growth supplement (Thermo Fisher Scientific) and 1% L-Glutamine (Thermo Fisher Scientific). Media changes were performed every 48 h until 80% confluency was reached, after which, the cells were enzymatically harvested (TrypLE Express, Gibco, Thermo Fisher Scientific) followed by centrifugation at 200 g for 5 min to obtain a cell pellet. The supernatant media was replaced by appropriate amount of warm (37°C) GelMA solution followed by gentle pipetting to constitute the GelMA bioink at 1×10⁶ cells/ml. The bioink was maintained at 37°C for 15 min before commencing further experiments.

2.7 Assessment of morphology of encapsulated cells and the hydrogel constructs

The morphology of hASC and 3T3 cells encapsulated within different groups of GelMA hydrogel constructs was assessed over a week in culture. To create each construct, 250 µl of the warm GelMA bioink was added and homogeneously distributed within a well of an untreated 24-well plate (VWR International, Radnor, PA) and thermally and photo-crosslinked at different combinations of pre-photo-crosslinking temperature (warm, ambient, cold) and UV exposure duration (4 s, 6 s, 8 s, 10 s). The constructs (n = 3 per group) were cultured (37°C, 5% CO₂) for a week with media changes every 24 h.

During the week in culture, the constructs were imaged via phase contrast imaging (DM IL LED FLUO, Leica Microsystems, Wetzlar, Germany). At Day 7, the constructs within the 24-well plates were fixed in 1 ml of 10% neutral buffered formalin (ShandonTM Formal-FixxTM, Thermo Fisher Scientific). The plates were then covered by Parafilm® (Millipore Sigma) and maintained at 22°C for 24 h, followed by washing thrice with PBS and stored overnight at 4°C in 3 ml PBS buffer containing 0.4% Triton-X (MilliporeSigma). Next, 3 ml of PBS buffer containing 100 μl

Phalloidin and 100 µl NucBlue (ThermoFisher Scientific) was added, and samples maintained under ambient conditions (22°C) for 2 h before confocal imaging (Fluoview 3000, Olympus, Tokyo, Japan). The average cell length was measured using FIJI³³ (n = 3 images per construct; n = 9 images per group), similar to a previous study³⁴. In addition, the hydrogel constructs were carefully extracted from the 24-well plates, and their macroscopic images captured using a dissection microscope (Leica Microsystems, Wetzlar, Germany), followed by determining the size of the hydrogels (i.e., the area covered by the hydrogel within the 2D images) via FIJI³³.

2.8 Quantitative real time PCR (qRT-PCR) of hASC encapsulated within GelMA

To study the effects of processing conditions on the gene expressions of the encapsulated hASC, GelMA hydrogel constructs of select groups (warm-4 s, cold-4 s, warm-10 s) were fabricated following the protocols described in section 2.7 and cultured (37°C, 5% CO₂) for 48 h. In parallel, hASC were cultured in treated 24-well plates (VWR International) at the same seeding density (250,000 cells/well) to serve as controls. To harvest the cells from the constructs, the supernatant media was removed after 48 h and replaced with 1 ml of 0.25% trypsin-EDTA. After 5 min of proteolytic degradation, the contents within each well were vigorously pipetted to ensure cell detachment from the matrix, and 1 ml of hASC media was added to neutralize the trypsin. The contents were then passed through a 40 µm cell strainer (FalconTM, Thermo Fisher Scientific), followed by centrifugation of the flow-through at 200 g for 5 min to obtain a cell pellet for the sample. The supernatant media was then removed, and the cells were resuspended in 1 ml of PBS and centrifuged again.

Total RNA was isolated from cells using RNeasy kit (Qiagen, Hilden, DE), and the RNA sample was treated with DNase following manufacturer instructions of Turbo DNA-free kit

(AM1907, Thermo Fisher Scientific). RNA concentrations were measured using nanodrop (Thermo Fisher Scientific). This was followed by cDNA synthesis from the DNA-free RNA sample using AffinityScript Multiple Temperature Reverse Transcriptase Kit (Agilent technologies, Santa Clara, CA). PCR primers designed for each gene (Table 2) were validated by amplifying using polymerase chain reaction (PCR) followed by gel electrophoresis with 1~2% agarose in TAE buffer. Following manufacturer's description of iQTM SYBR® Green Supermix (Bio-Rad laboratories, Hercules, CA), qRT-PCR was performed with initial denaturation at 95°C for 3 min followed by 40 cycles of denaturation at 95°C for 15 s and annealing at 60°C for 30 s. Melt-curve analysis was followed to confirm that no non-specific amplification occurred. The mRNA expression level of each target gene was normalized to that of the reference gene GAPDH³⁵.

Table 2. Primers for select gene expressions of human adipose stem cells (passage 2)

Name	Gene-type (with reference)	Sequence
GAPDH fwd	Reference (housekeeping) gene ³⁵	AAGGTGAAGGTCGGAGTCAACG
GAPDH rev	Reference (nousekeeping) gene	AGGTCAATGAAGGGGTCATTGATGG
CD44 fwd	Stem cell marker ²²	AGATGGAGAAAGCTCTGAGCATCG
CD44 rev	Stem cen marker	TGTTTGCTGCACAGATGGAGTTG
ICAM-1 fwd	Intercellular adhesion and proinflammatory marker ²³	CGGCCAGCTTATACACAAGAACC
ICAM-1 rev		ATTTTCTGGCCACGTCCAGTTTC
ITGA1 fwd	Cell-matrix interaction ²⁴	TCTACCAAAAAGAATGAACCGCTTGC
ITGA1 rev	Cen-matrix interaction-	ATGATTGTACCGAGGCTGTCCAG
ITGA10 fwd	Cell-matrix interaction ²⁵	TGTTCTTGCCCCTGGTGTTC
ITGA10 rev	Cen-matrix interaction-	TGTCCACCCCAACATGTTG

2.9 Ultrasound-assisted biofabrication of GelMA constructs with cell patterning

To assess key characteristics of select groups of thermally and photo-crosslinked GelMA constructs (warm-10 s, cold-6 s; n = 3 per group) for biomimetic tissue engineering applications,

constructs with anisotropically organized hASC were fabricated via UAB^{8,26,27} – a hybrid process¹⁶ capable of rapid and controllable patterning of cells within biomatrices, highly relevant to the engineering of soft tissues such as ligaments, tendons, and cardiac muscle. The UAB setup comprised of a non-treated petri dish (MilliporeSigma) with an attached transducer-reflector pair. The plate-type piezoelectric transducer (resonant frequency 2 MHz, Steiner and Martins Inc., Davenport, FL) and the reflecting glass coverslip (18×18×0.2 mm³) were attached opposite each other with a separation of 21 mm. The transducer was connected to an amplifier (240L, Electronics & Innovation Ltd., Rochester, NY) that received source signal from a function generator (Keysight Technologies Inc. Santa Rosa, CA).

To create the warm-10 s constructs (n = 3), the UAB setup was placed on top of the UV lamp (405 nm, 10 mW/cm² at the bioink interface) with an opaque mask containing a 20×20 mm² transparent opening positioned in between the lamp and the petri dish. 2 ml of warm GelMA bioink containing 1×10^6 hASC/ml was dispensed into the petri dish and the transducer actuated by a voltage signal comprised of 1 s bursts followed by 1 s pauses at 2 MHz and 50 Vpp, which has been previously demonstrated to be non-deleterious to cells ($\sim100\%$ cell viability)⁸. Actuation of the transducer resulted in the formation of a standing bulk acoustic wave (SBAW) with planar pressure nodes parallel to the walls of the transducer within the bioink²⁶ due to the interference of the incident and reflected waves. The resulting acoustic radiation force caused the cells to organize along arrays representing the planar nodes of the SBAW; as per established theory, the arrays are separated by an integer multiple of half the wavelength (i.e., theoretical inter-array spacing = λ 2). The bioink was photo-crosslinked (10 s of UV exposure) after 1 min of transducer actuation, while the transducer remained actuated for 5 min. The crosslinked hydrogel construct was transferred to

an untreated petri dish (Ø 35 mm) and cultured (37°C, 5% CO₂) in 4 ml of hASC media for a week. Media changes were performed every 48 h.

To create the cold-6 s constructs (n = 3), the UAB setup was first placed in a cold (10°C) water bath. Then, the warm bioink was introduced and the transducer actuated (1 s bursts – 1 s pauses at 2 MHz and 50 Vpp) for 5 min, during which time, the bioink underwent thermal crosslinking. After 5 min of ultrasound actuation and thermal crosslinking, the UAB setup was transferred onto the top of the UV lamp, followed by selective photo-crosslinking (6 s of UV exposure) of the bioink through the mask. The setup was then placed within a larger petri dish (Ø 100 mm) and incubated (37°C, 5% CO₂) for 30 min to liquefy any uncrosslinked GelMA that was then aspirated. The crosslinked hydrogel construct (20×20×1.5 mm³) was then transferred to an untreated 6-well plate and cultured in 4 ml of hASC media for a week with media changes every 48 hours.

For both groups, constructs fabricated using the same UAB setup and crosslinking protocols but without ultrasound actuation, and hence, no cell patterning, were included as controls. At the end of the week, all constructs were stained for live/dead assay (Life Technologies, Carlsbad, CA), followed by fixation in 4 ml of 10% neutral buffered formalin and staining using phalloidin and NucBlue as described in section 2.7. Cell length and the inclination angle of the cells with respect to the aligned arrays (y-axis) was determined (n = 3 images per anisotropic construct, n = 9 images per group) using FIJI as described previously³⁴.

2.10 Statistical analysis

Statistical analysis was performed in JMP[®] (SAS, Cary, NC) at significance level of $\alpha = 0.05$ using a three-way ANOVA (compression testing) or two-way ANOVA (microstructural, proteolytic

degradation, and anisotropic construct analyses) with Tukey HSD post hoc tests. In the qPCR study, the effects of different matrix formulations on specific gene expression were compared using Student's t-tests.

3. Results

3.1 Mechanical properties of GelMA hydrogels

The results of uniaxial compression testing of the GelMA constructs of different compositions fabricated under different processing conditions are presented in **Figure 2**. The compressive elastic modulus (i.e., stiffness) of the hydrogels was significantly affected by GelMA composition, prephoto-crosslinking solution temperature, and UV exposure duration (p < 0.0001). The interactions of UV exposure duration with the composition and solution temperature were also significant (p < 0.05). Post hoc analysis (**Table S1**) showed that the hydrogel stiffness was higher when the prephoto-crosslinking solution temperature was lower, which indicates a higher density of packing of polypeptide networks during thermal crosslinking (illustrated in **Figure 1**). Furthermore, the hydrogel stiffness increased with increasing UV exposure duration, which can be attributed to a greater number of covalent bonds forming between the methacrylate groups.

Higher stiffness was noted in hydrogels of higher GelMA concentration because of increased presence of polymeric chains that could be thermally or photo-crosslinked. Higher DOS also resulted in stiffer hydrogels due to increased presence of moieties that could be covalently bound upon UV exposure. As such, doubling the GelMA concentration had a greater impact on the stiffness than doubling the DOS, in that, the 40% DOS – 10% w/v formulation was stiffer than the 80% DOS – 5% w/v one. This signifies that higher packing density of polymers in the hydrogel has a higher contribution to stiffness compared to the amount of crosslinkable groups.

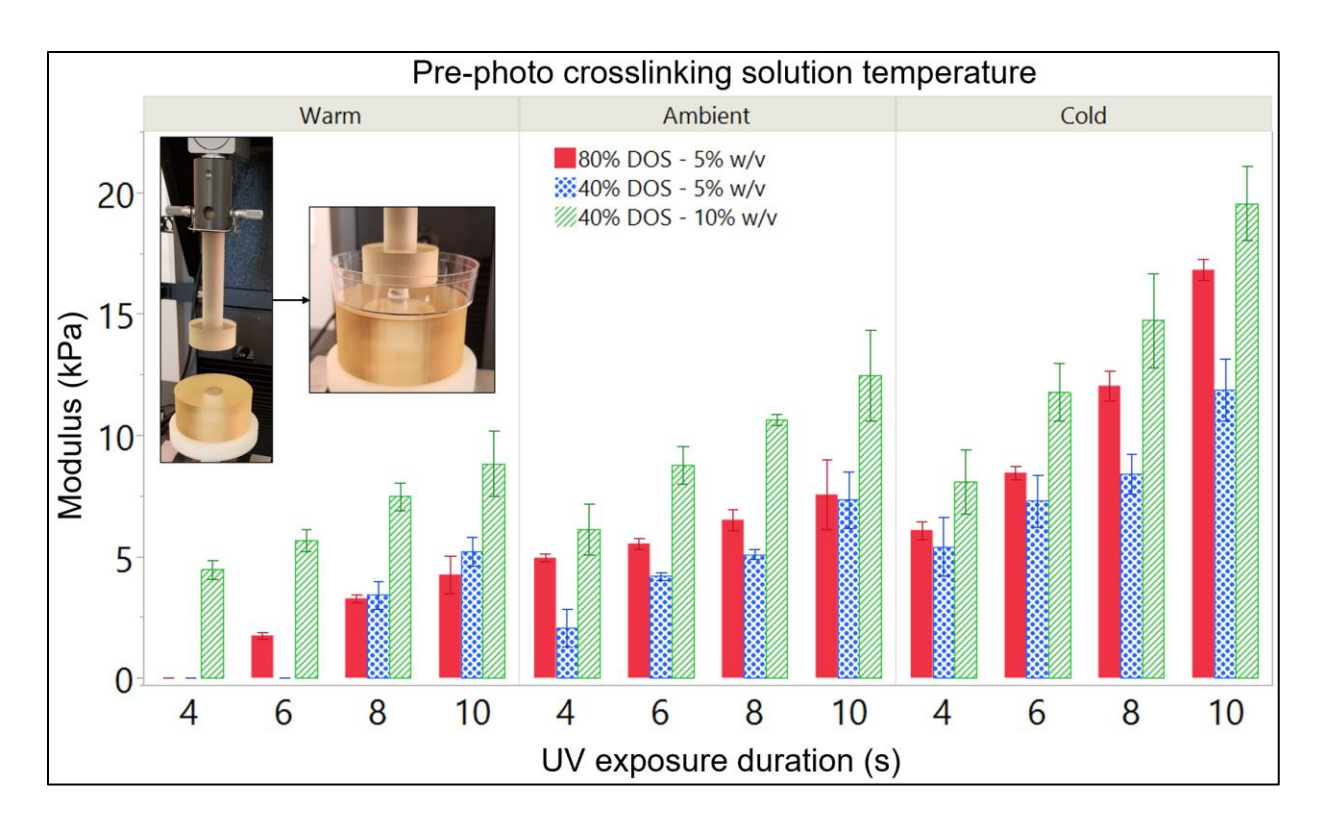


Figure 2. Results of uniaxial compression testing (setup shown in the inset images) of GelMA hydrogels. The modulus of hydrogels was higher at lower pre-photo-crosslinking solution temperature, greater UV exposure duration, and higher degree of methacrylate substitution and GelMA concentration. Post-hoc analysis can be found in supporting information (**Table S1**).

The broadest range of stiffness was reported in the 80% DOS – 5% w/v hydrogels. For the same degree of thermal and photo-crosslinking, the lowest stiffness of 80% DOS – 5% w/v hydrogels (0.25 kPa) was similar to that of the 40% DOS – 5% w/v group (p > 0.05), and their highest stiffness (17 kPa) was similar to that of the 40% DOS – 10% w/v group (p > 0.05) (**Table S1**), respectively. Therefore, all further studies were conducted with the 80% DOS – 5% w/v formulation.

3.2 Microstructural analysis of GelMA hydrogels

Figure 3(a) shows representative CryoSEM images highlighting the microstructure of different GelMA hydrogel groups. The results of porosity and pore size for each group determined via a custom MATLAB algorithm are presented in **Figure 3(b)**. Both porosity and pore size were significantly affected by the interaction of pre-photo-crosslinking solution temperature and UV exposure duration (p < 0.0001).

Decreasing the temperature of GelMA before photo-crosslinking induced tighter entanglement of polypeptide networks, which is evident from a closer examination of the microstructure of the ambient and cold hydrogel groups (Figure 3(a)). Herein, increasing the UV exposure duration increased the number of covalent bonds between methacrylate groups, thereby reducing porosity and pore size (Figure 3(b)). There was also a direct correlation between the pore sizes and the compressive elastic moduli in that the stiffer hydrogel groups possessed smaller pores and lower porosity (Figure 3(b)). Irradiating these thermo-reversibly crosslinked hydrogels via UV in the presence of the LAP photoinitiator resulted in covalent bonding between the methacrylate groups in neighboring polypeptide chains, thereby irreversibly crosslinking the hydrogels.

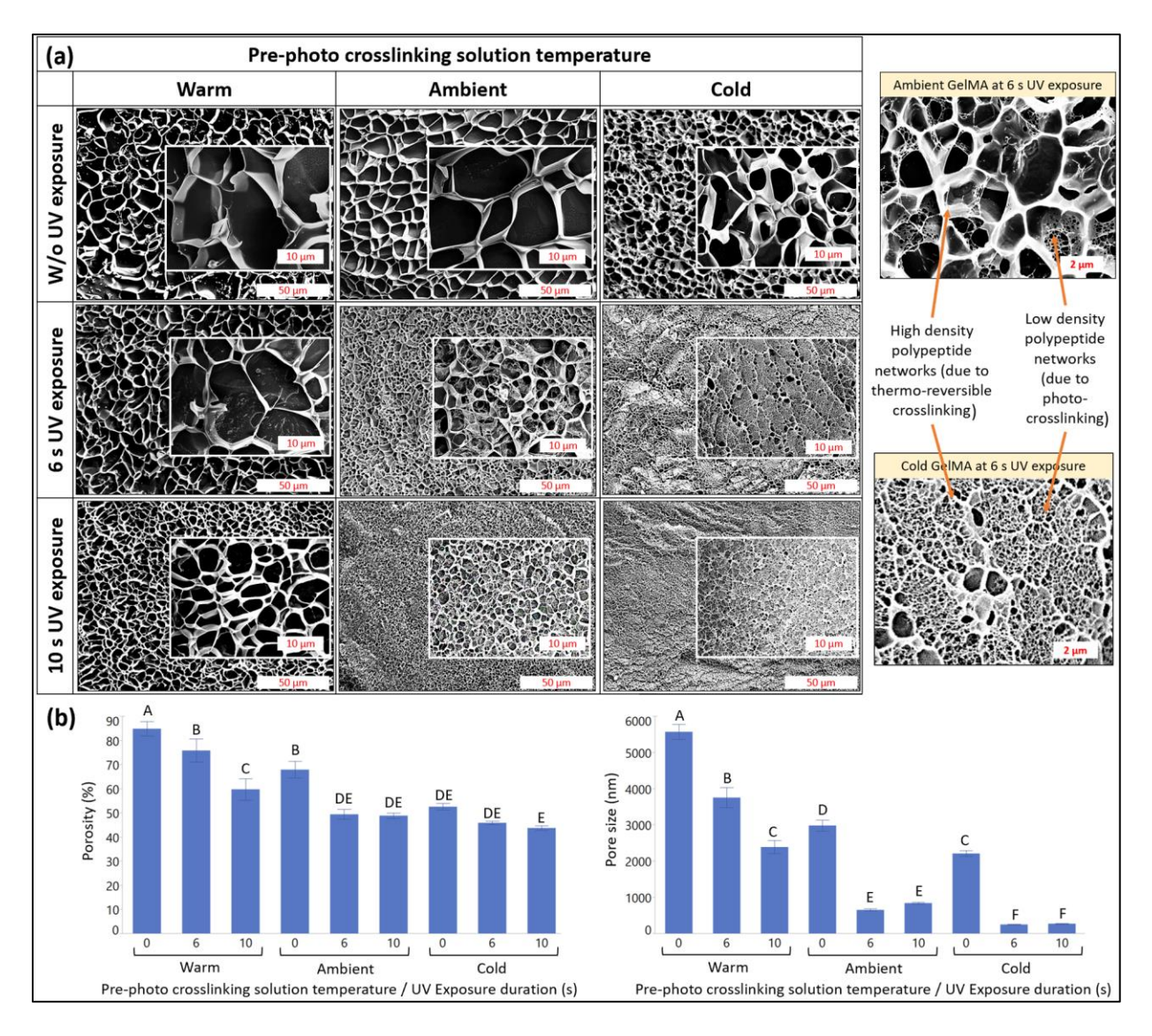


Figure 3. (a) CryoSEM images at 650X magnification (insets at 3500 X magnification) demonstrating the microstructure of GelMA hydrogels formulated at varying pre-photo-crosslinking solution temperatures and photo-crosslinking durations. Hydrogels formulated solely by thermal crosslinking (without UV exposure) were included to enable clear comparisons between thermally and photo-crosslinked microstructures. Greater entanglement of polypeptide chains is evident in the microstructure in which subsequent photo-crosslinking created covalent bonds in between the polypeptide chains, leading to an irreversibly crosslinked matrix. **(b)** MATLAB image analysis and results of porosity (left) and pore size (right) of various GelMA hydrogel formulations. Both porosity and pore size were lower at lower pre-photo-crosslinking solution temperature and higher UV exposure duration (p < 0.0001). Connecting letters

from post hoc analysis are shown above the bars. Groups not having at least one common letter are statistically significantly different from one another (p < 0.05).

3.3. Proteolytic degradation of GelMA hydrogels

The effects of thermal and photo-crosslinking conditions on proteolytic degradation characteristics of select GelMA hydrogel groups are summarized in **Figure 4**. As postulated from the compressive stiffness and microstructure results, the degradation rate (slope of the curve) was faster at higher pre-photo-crosslinking temperature and lower UV exposure duration (p < 0.0001). These results indicate that inducing some degree of thermal crosslinking in the GelMA matrix prior to photo-crosslinking can prolong the hydrolysis within the GelMA matrices. This will be highly beneficial during long-term in vitro and in vivo applications of GelMA hydrogels³⁶.

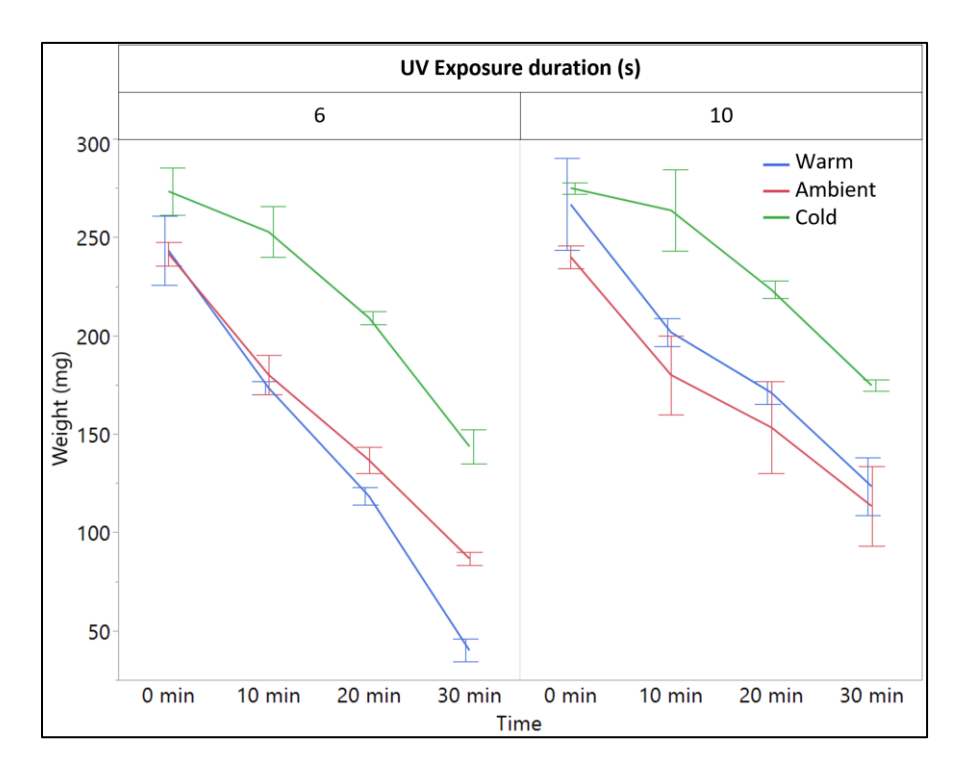
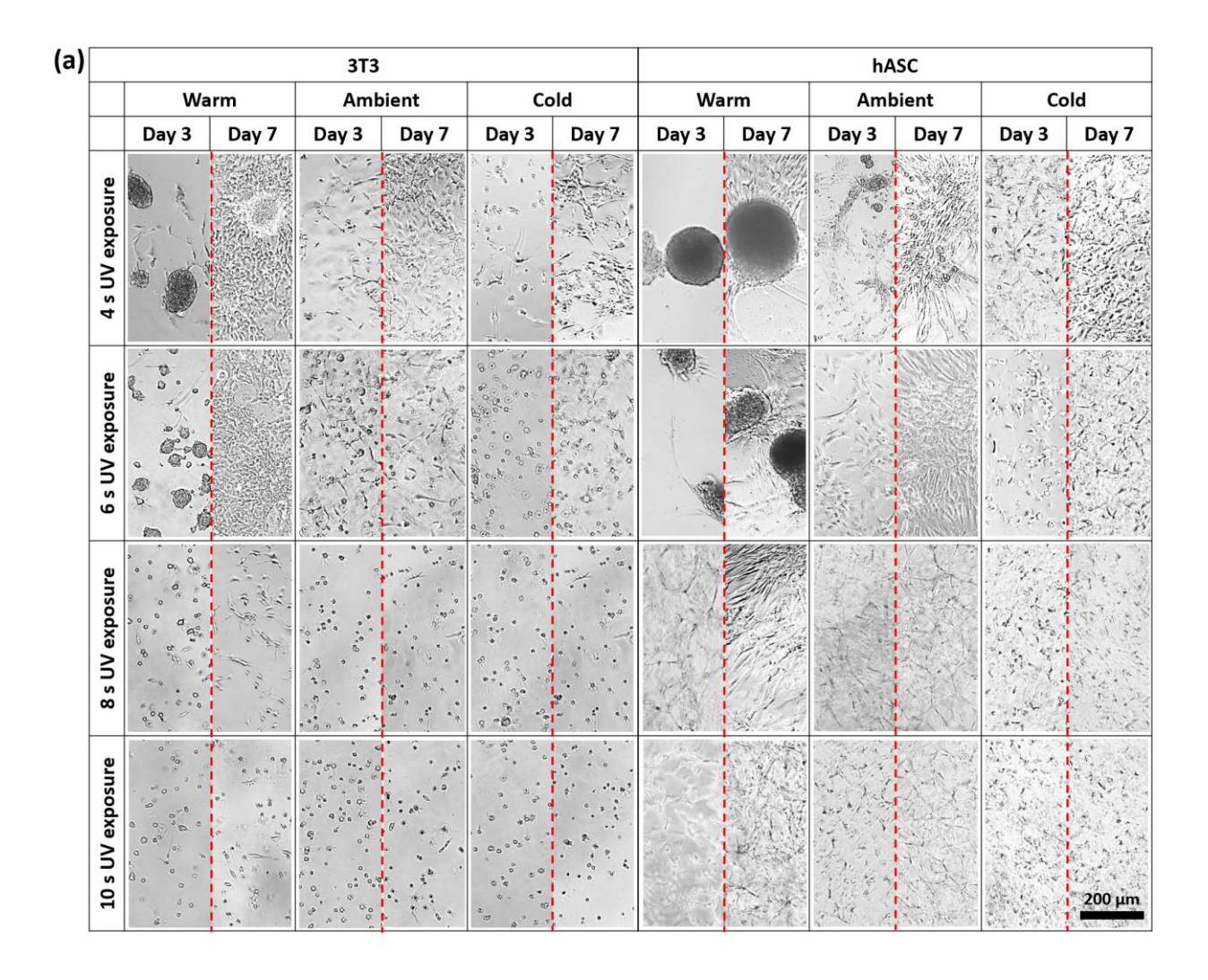


Figure 4. Trypsin-induced proteolytic degradation of GelMA hydrogels over time. The degradation rate decreases by reducing the initial solution temperature or increasing the UV exposure duration.

3.4. Encapsulated cell morphology and hydrogel construct fidelity over a week in culture

Figure 5 shows the results of cell and construct morphology of different GelMA formulations during a week in culture. Micrographs demonstrating hASC and 3T3 cell morphology evolving over the week in culture are shown in **Figure 5(a)**, and the corresponding analysis for the length of cells is shown in **Figure 5(b)**. The length of the cells was significantly affected by the interaction of pre-photo-crosslinking solution temperature and UV exposure duration (p < 0.0001).



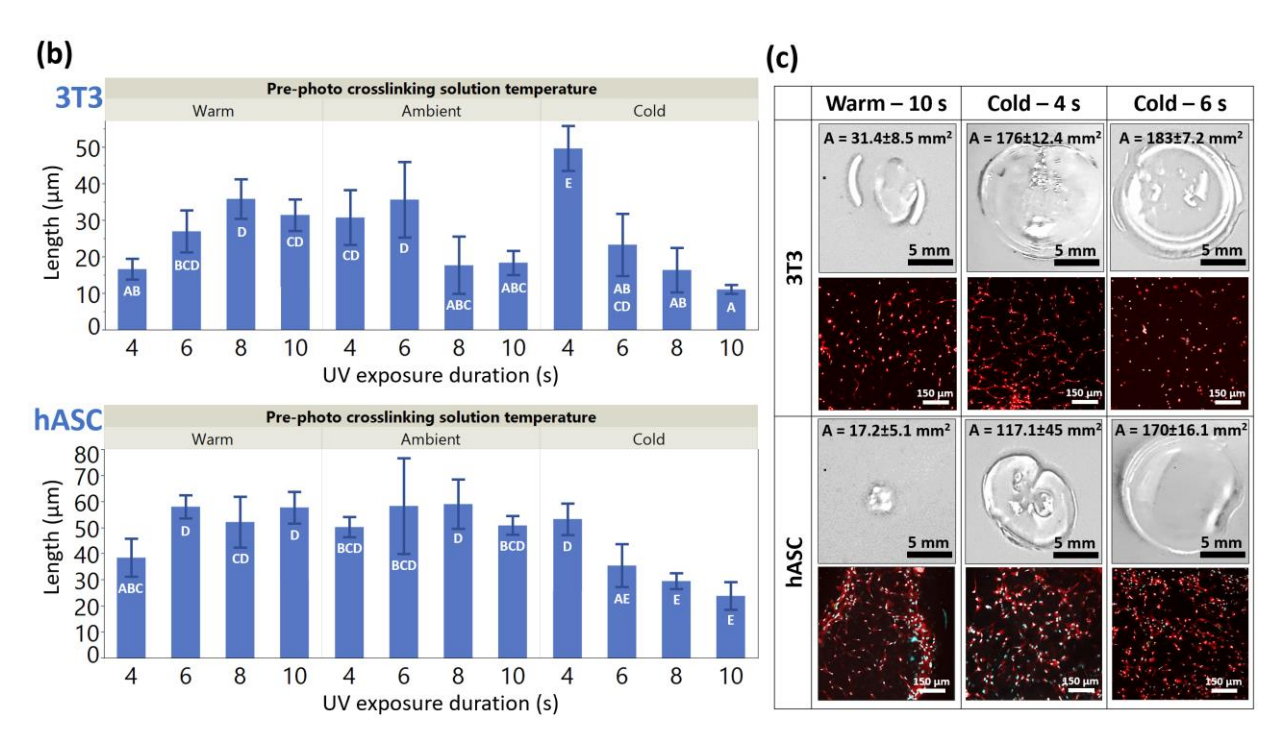


Figure 5. (a) Micrographs showing the behavior of 3T3 cells and hASC encapsulated in various GelMA formulations over a week in culture. The 3T3 cells formed spheroids in low stiffness hydrogels, with larger spheroids observed at the lowest stiffness. In moderate stiffness hydrogels, cells proliferated throughout the constructs, with higher cell attachment and proliferation noted in groups subject to higher degree of thermal crosslinking (ambient-4 s and 6 s, and cold-4 s). Cell elongation and proliferation were thwarted in the high stiffness groups (ambient-8 s and 10 s, and cold-6 s, 8 s, and 10 s). Scale bar (bottom right) is common for all the images. Compared to 3T3 cells, the hASC demonstrated better adherence to the matrix than 3T3 cells. Spheroid formation and better cell proliferation throughout 3D hydrogels were observed over a wider range of GelMA formulations. Scale bar (bottom right) is common for all the images. (b) Length of the 3T3 cells and hASC within different GelMA formulations, which is dependent on the interaction of the prephotocrosslinking solution temperature and the UV exposure duration (p < 0.0001). Collective analysis of the stiffness and length measurements demonstrates that a stiffness in the range of 2-6 kPa is ideal for an elongated cell morphology. Within this range, the cells are more elongated in the presence of entangled polypeptide networks due to thermal crosslinking, as is in the case of cold-4 s constructs with 3T3 cells. Connecting letters from post hoc analysis are shown above the bars. Groups not having atleast one common

letter are statistically significantly different from one another (p < 0.05). (c) Macroscopic images and micrographs (blue: nucleus, red: actin) of select GelMA formulations with 3T3 cells and hASC after a week in culture. Comparison between warm-10 s and cold-4 s formulations that have similar stiffness (p > 0.05) shows that increasing the entanglements of polypeptide chains through thermal crosslinking prior to photocrosslinking improves matrix fidelity over time. Increasing the UV exposure duration can further improve matrix fidelity, as is evident from comparison between cold-4 s and 6 s groups. Overall, hASC, being more contractile than 3T3 cells, led to greater matrix deformation over time.

Considering these cell length results in conjunction with the hydrogel stiffness analyses (Figure 2), it is evident that an optimal stiffness is needed to elicit cell elongation within the hydrogels. For 3T3 cells, the mean cell length was the highest and comparable (i.e., not statistically significantly different) at 6, 8 and 10 s of UV exposure within warm formulations, at 4 and 6 s of UV exposure within ambient formulations, and at 4 s of UV exposure within cold formulations. The stiffness of these six formulations ranges from 2-6 kPa. Across these, the 3T3 cells were the most elongated within the cold-4s formulation, despite this formulation possessing the highest mean stiffness among the group. A similar trend was noted with the hASC, except that the hASC demonstrated elongation in all the ambient formulations. A more elongated cell morphology of hASC and 3T3 cells in the ambient and cold GelMA formulations, despite the higher mean stiffness in these groups compared to the warm formulations, could be attributed to the presence of tighter crosslinking sites resulting from the initial thermo-reversible crosslinking, which could emulate the structure of collagen^{1,9}. This indicates that the introduction of moderate degree of thermal crosslinking in the GelMA matrix prior to photo-crosslinking facilitates cell adhesion. It should also be noted that in the hydrogels with the highest stiffness (cold-8 s and cold-10 s), the cells could not remodel the surrounding GelMA matrix and exhibited a less elongated morphology.

This trend in stiffness-cell morphology relationship is consistent with literature^{37,38}. At very low stiffness (warm-4 s and warm-6 s), formation of cellular spheroids was observed in groups with the lowest compressive stiffness (**Figure 5(a)**). This is because it was easier for the contractile fibroblasts to shear through the hydrogel matrix and clump together into distinct spheroids. The spheroids were larger in the groups subject to 4 s of UV exposure, which could be attributed to the greater compliance of the GelMA matrix at lower stiffness. Due to the higher degree of attachment and contractility, hASC also demonstrated spheroid formation in the ambient-4 s hydrogels.

Similar to the cell length, the morphology of cell-laden GelMA constructs (select groups shown in Figure 5(c)) after week in culture was also significantly affected by the interaction of pre-photo-crosslinking solution temperature and UV exposure duration (p < 0.0001). Looking collectively at the results of the construct morphology and the hydrogel stiffness (Figure 2), it is evident that despite having similar stiffnesses (p > 0.05, refer to the post hoc analysis in Table S1), the warm formulations demonstrate significantly higher matrix deformation (p < 0.05) compared to the cold formulations, which could be attributed to the absence of tighter crosslinked networks necessary to strengthen the matrix. Conversely, the cold hydrogels were more stable, physiologically. For hASC and 3T3 cells, the cold-6s and cold-4 s formulations were optimum, respectively, in that these allowed for cell elongation while exhibiting relatively lower matrix contraction. However, in case of hASC, cells exhibited less elongated morphology in the cold-6 s formulation compared to cold-4 s formulation (p < 0.05).

3.5 Gene expression of hASC encapsulated within GelMA hydrogels

Among the groups studied so far, the warm-10 s and cold-4 s groups had demonstrated similar stiffness (**Table S1**) and cell elongation (**Figure 5(b)**) but substantially different construct

morphology (**Figure 5(c)**) due to the presence of entangled polypeptide networks (**Figure 3**). In addition, the warm-4 s group possessed the lowest stiffness (**Figure 2** and **Table S1**). Therefore, it was deemed essential to compare the gene expressions between these groups. The results of qRT-PCR are presented in **Figure 6**.

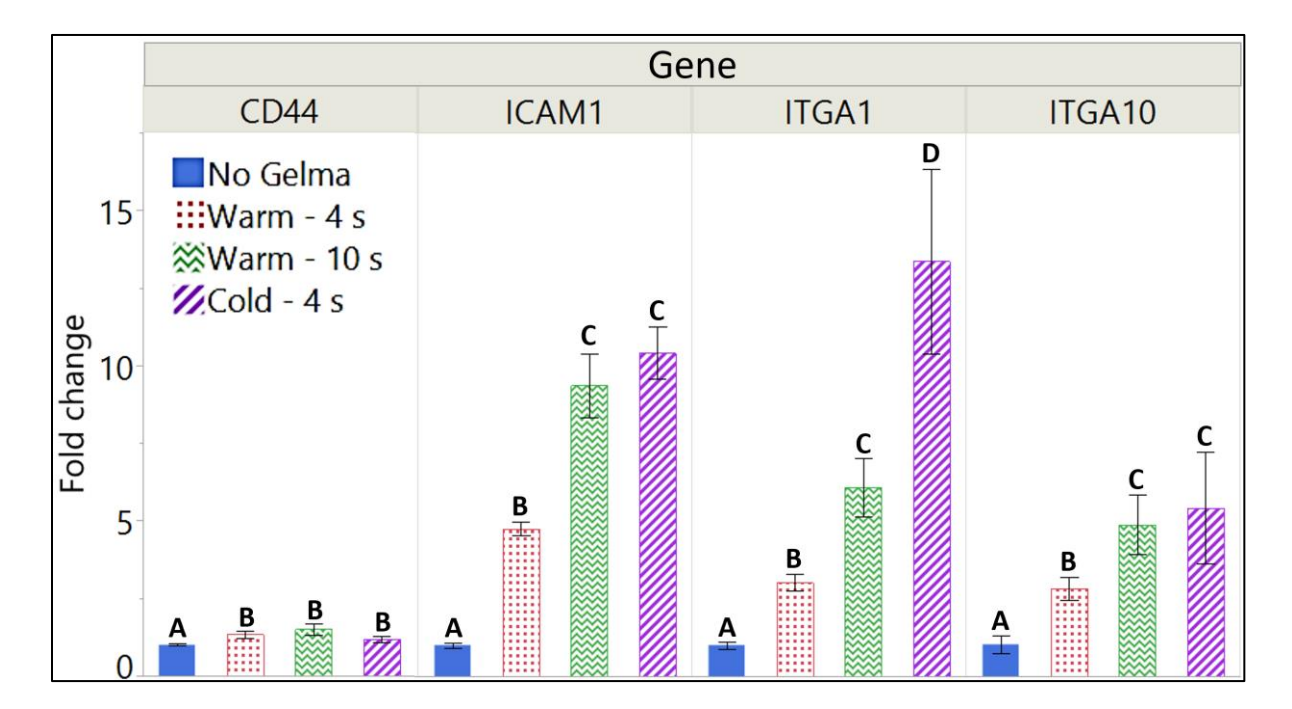


Figure 6. Results of qRT- PCR. Presence of GelMA matrix upregulated the stem cell marker CD44 (p < 0.05). In addition, as the matrix stiffness increased, there was substantial upregulation of pro-inflammatory marker, ICAM1, and cell-matrix interaction markers, ITGA1 and ITGA10. Connecting letters from post hoc analysis are shown above the bars. Groups not having atleast one common letter are statistically significantly different from one another (p < 0.05).

The results show that the presence of GelMA matrix facilitates maintenance of hASC stem potency as indicated by small (\sim 1.8 fold) yet significant (p < 0.05) increase in adipogenic stem cell marker – CD44. This indication of cell encapsulation in hydrogels facilitating preservation of stem cell potency is consistent with literature^{38,39}. In comparison, all the GelMA-containing groups

demonstrated a substantial increase (> 5 fold) in the expression of ICAM1, which is a cell-cell signaling marker that has been shown to be associated with pro-inflammatory immune responses⁴⁰. Such a response can be utilized advantageously in applications where a pro-inflammatory response is desirable. For example, GelMA patches containing encapsulated hASC could potentially be used to home macrophages and T-cells to a diseased site such as a cancerous tissue. On the other hand, in GelMA constructs that are intended for use as an implanted tissue substitute, an over expression of ICAM1 may result in excessive killing of encapsulated cells in the tissues through macrophage infiltration.

The GelMA hydrogels also demonstrated an upregulation of ITGA1 and ITGA10 that encode for collagen binding peptides. This is because the gelatin backbone in GelMA consists of similar adhesion peptide sequences that are found in collagen⁴¹. The upregulation of cell-matrix interaction was higher at higher matrix stiffnesses. Of note, although the matrix stiffness of warm-10 s and cold-4 s groups is similar, upregulation of ITGA1 gene in cold-4 s constructs compared to warm-10 s constructs demonstrates that the presence of entangled polypeptide chains in cold-4 s leads to an improved cell-matrix adhesion. In such a scenario, introducing some degree of thermal crosslinking in the matrix prior to photo-crosslinking could improve the cell adhesion characteristics. At higher stiffness, although there is upregulation of pro-inflammatory marker ITGA1, molecular or materials strategies can be considered to prevent homing of immune cells. For example, blocking the interaction of ICAM1 with its ligand⁴⁰, lymphocyte function-associated antigen 1 (LFA1), or hybridization with other immune-isolative materials such as alginate⁴², can be used as effective tools to prevent migration of immune cells to the implanted GelMA-based tissue.

Depending upon the desired application of the hydrogels and the encapsulated cell type, future studies can investigate the effects of GelMA matrix characteristics on the upregulation of genes related to the differentiation of hASC^{43,44}, or other functional characteristics such as ECM production⁴⁵ and extracellular vesicle secretion⁴⁶. Herein, transcriptomic profiling via RNA-Seq could also reveal a wider gambit of changes to the gene expression of the encapsulated cells⁴⁷.

3.6. Demonstration of the need to understand the critical process-structure-function interactions:

A use-case for hybrid biofabrication using GelMA hydrogels

Results so far have demonstrated how synergistic thermal and photo-crosslinking under appropriate processing conditions can lead to more functional GelMA hydrogels. As per the results and discussion in section 3.4, cold-6 s formulation resulted in the most stable hydrogel with good hASC elongation, while the warm-10 s formulation allowed for significant matrix remodeling that could be beneficial for cell elongation and proliferation. Hence, hydrogels of these two groups were investigated for engineering anisotropic constructs featuring uniaxial cell organization via UAB (Figure 7(a)).

The results of cellular responses and morphology of constructs fabricated via UAB and cultured over a week are summarized in **Figure 7(b)**. As expected, the anisotropically patterned hASC in the warm-10 s group significantly molded the hydrogel matrix and established cell-cell contacts and elongated morphologies along the principal direction of alignment of cellular arrays. Over a week in culture, the cells proliferated predominantly along the principal direction of the arrays, as indicated by the angular orientation of the cells, which primarily lies within $\pm 45^{\circ}$ with respect to the array (y-axis). However, this creation of anisotropy was accompanied by significant reduction in the size of the hydrogel constructs (p < 0.05), and a reduction in the spacing between

the neighboring arrays of cell (i.e., a reduction in the inter-array spacing, p < 0.05). In contrast, in the cold-6 s group, the cells were unable to establish the relevant cell-cell contacts and proliferated isotropically over time, thereby losing the desired anisotropic organization, which could be attributed to the limited compliance of the matrix and inhibited cell elongation. However, the low matrix compliance ensured that the size of the hydrogel constructs and inter-strand spacing was not significantly affected (p > 0.05).

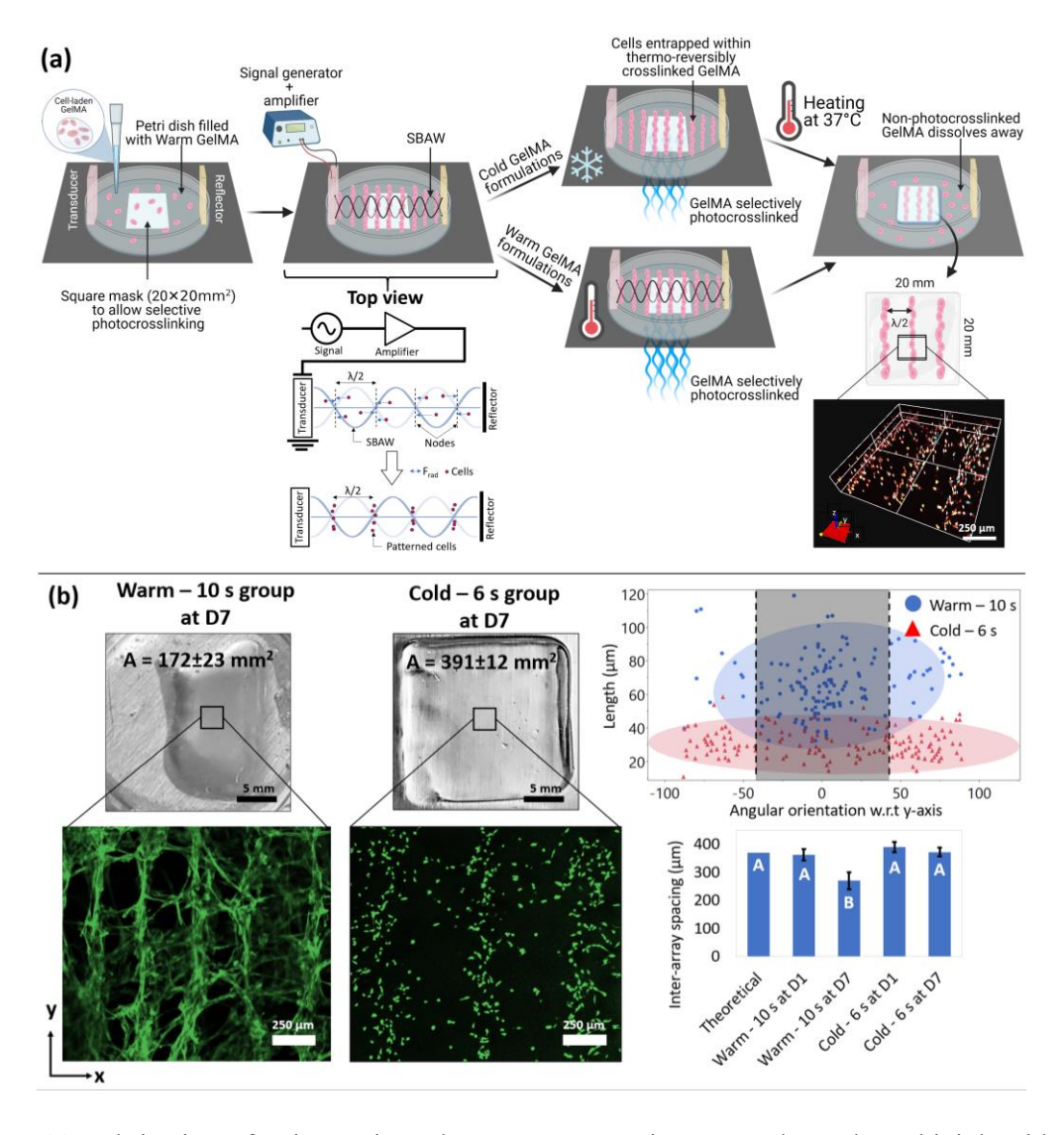


Figure 7. (a) Fabrication of anisotropic GelMA constructs via UAB. The GelMA bioink with cells is dispensed within the UAB setup, and a SBAW is generated within the bioink upon actuation of the

transducer. The resulting acoustic radiation forces acts on the cells to organize them along pressure nodes separated by half the wavelength of the applied ultrasound (i.e., the theoretical inter-array spacing $(\lambda/2)$). The GelMA is then either directly photocrosslinked (for warm GelMA formulations) or allowed to thermoreversibly crosslink prior to photocrosslinking (for cold GelMA formulations). After photocrosslinking, the petri dish is heated to 37°C (for cold GelMA formulations only, since warm GelMA formulations are already at 37°C), due to which, any non-photocrosslinked GelMA can be easily aspirated away, leaving behind the GelMA construct with anisotropically patterned cells. The representative confocal image on the right demonstrates prevalence of cell (hASC) patterning along the thickness of the construct. (b) Live/dead (L/D) analysis demonstrates 100% hASC viability in all groups after a week in culture. The warm-10 s formulation allowed for significant matrix remodeling, leading to enhanced cell elongation (higher length) and alignment (angle within ±45° w.r.t the strand (y-axis)) along the patterned strands, albeit with significant matrix contraction (p < 0.05) and reduction in the inter-array spacing (p < 0.05). In contrast, the cold-6 s formulation demonstrated lesser degree of cell elongation and alignment, but better construct fidelity and maintenance of inter-array spacing over a week in culture due to more restrictive matrix remodeling. Connecting letters from post hoc analysis are shown above the bars. Groups not having atleast one common letter are statistically significantly different from one another (p < 0.05).

Although the cells in the cold-6 s group did not exhibit elongation along the principal direction of the strand, the density of cell packing may be an important factor to consider here. The process of cell patterning in UAB is gradual, in that cells traversing to the nearest pressure node under the action of acoustic radiation forces also experience viscous drag forces that resist their motion²⁷. In cold GelMA formulations, the thermal crosslinking of the matrix is occurring concomitantly with the ultrasound-driven movement of the cells to their nearest SBAW pressure nodes. This leads to an increase in the matrix viscosity and drag forces on the cells, resulting in a lower degree of cell packing in aligned cellular strands at the pressure nodes, as seen in **Figure**

7(b) ²⁶. The reduction in the establishment of cell-cell contacts thereby affects cell proliferation along the principal direction of the strand. In such scenarios, several UAB design and process parameters can be optimized²⁷. For example, reducing the separation between the transducer and reflector, increasing the duration of transducer actuation, and increasing transducer vibration amplitude can result in higher cell packing density along aligned strands while preserving cell viability. Optimizing such process characteristics to allow cell elongation while maintaining construct fidelity will be in the scope of our future work.

4. Discussion

GelMA hydrogels are increasingly being used for a variety of biomedical applications owing to their suitable biocompatibility and chemical properties including reversible thermal crosslinking and covalent photocrosslinking, which allow tunability of their physical characteristics. This work aimed at elucidating the critical material-process-structure-function interrelationships, which can aid in future research to appropriately tune hydrogel characteristics for their desired applications.

In the first phase, the effects of two key processing parameters (pre-photocrosslinking solution temperature and UV exposure duration) and GelMA composition (concentration and degree of substitution) on the matrix stiffness was investigated. Herein, the range of observed stiffnesses of the hydrogels spanning the three GelMA compositions fabricated under different processing conditions is relevant to a variety of tissues⁴⁸. For example, the stiffness of warm hydrogels that did not undergo thermal crosslinking prior to photo-crosslinking is similar to the stiffness of very soft tissues such as brain, thymus, and pancreas (0.25 – 5 kPa), whereas the ambient and cold hydrogels that were subject to some degree of thermal crosslinking possess stiffness similar to that of iris, lung, spleen, and liver (5 – 15 kPa). In future, it is possible to create

hydrogels possessing even higher stiffnesses by altering GelMA composition or increasing the extent of thermal and photo-crosslinking, which would be relevant for orthopaedic tissue engineering applications as well as tumor-based cancer or fibrotic disease models¹.

The same concentration of photoinitiator was used across all hydrogel formulations in this work. But it should be noted that the photoinitiator concentration can impact the hydrogel stiffness^{1,11} by altering the amount of free radicals present to initiate photopolymerization. For example, for a given set of material composition and processing conditions, increasing the photoinitiator concentration will result in creation of more free radicals, thereby leading to an increase in photocrosslinking density and hydrogel stiffness⁴⁹. In future, once the extent of thermal and photo-crosslinking has been optimized for a given application as per the framework described in this work, the amount of photoinitiator concentration can be optimized as per Beer-Lambert law for modeling the photoinitiation kinetics or by introducing UV-absorptive dyes within the GelMA formulation, to precisely control the extent of photo-crosslinking^{50,51}. This can help achieve the desired degree of photo-crosslinking while avoiding any additional crosslinking with subsequent UV exposure.

The microstructure (**Figure 3**) and cell and construct morphology assessment (**Figure 5**) studies in this work focused on a single composition of GelMA (80% DOS – 5% w/v). These characteristics will vary by composition. A formulation with higher GelMA concentration would provide more attachment moieties for the cells, but the increased matrix density would further limit matrix remodeling and cell elongation. In this scenario, the amount of thermal crosslinking can be increased by reducing the pre-photo-crosslinking solution temperature. Using a lower DOS matrix, in conjunction, can reduce the subsequent extent of photo-crosslinking. Future studies can characterize the relationships between matrix concentration and DOS, processing conditions

(degrees of thermal and photo-crosslinking), and key functional responses of cells (e.g., stem cell phenotype, differentiation, and preservation of anisotropy over time) following the framework herein.

Results of the morphology of 3T3 cells and hASC (Figure 5(a,b)) and their corresponding constructs (Figure 5(c)) showed that the matrix stiffness and microstructure needs to be optimum to allow for cell elongation, proliferation and the maintenance of construct fidelity. For example, for hASC, in comparison to 3T3 cells, a GelMA hydrogel with higher stiffness and degree of thermal crosslinking was more appropriate to ensure maintenance of construct fidelity, while allowing the cells to elongate and proliferate within the matrices. Future studies on different cell types could perform similar screening experiments to those outlined in the present work, to find out the optimal thermal and photo-crosslinking modalities during processing. Furthermore, the differences in cell behavior due to differences in matrix microstructure and stiffness have relevance to different applications of GelMA including tissue engineering. Applications that require significant matrix remodeling (such as cardiac tissue development) or cell elongation to generate cell-cell synapses (such as smooth muscle formation) would benefit from a more compliant matrix, in which case, inducing lesser degree of thermal crosslinking may be beneficial^{34,52}. However, most biofabricated soft tissues such as tendons, ligaments and cardiac muscle require prolonged culture in a bioreactor, preferably under perfusion and dynamic loading conditions^{52,53}. Herein, less stiffer hydrogels such as the warm-10 s formulation are likely to degrade or rupture under the dynamic culture conditions. This has direct relevance to the anisotropic tissue biofabrication approach highlighted in Figure 7. Herein, along with a balance of thermal and photo-crosslinking to promote matrix longevity, the packing density of the cells along the arrays (Figure 7) would also need to be optimized (e.g., by appropriately increasing the SBAW pressure or ultrasound

exposure duration) in order to establish the necessary cell-cell contacts to promote cell elongation along the arrays, eventually leading to matured tissue constructs with the desired shape-fidelity and anisotropic biomechanical characteristics.

Similarly, an optimal balance between the extent of thermal and photo-crosslinking may be desirable for delivery of therapeutics (e.g., drugs, cells, cell-derived exosomes, etc.) wherein the release of encapsulated cargo depends upon the rate of matrix degradation and swelling. Lower degree of thermal crosslinking would lead to higher rate of matrix degradation and swelling³⁶. As such, the thermal crosslinking and resulting matrix degradation and swelling properties would have to be optimized to match the desired rate of cargo delivery for a given therapeutic application³⁶.

In contrast, investigations into cell spheroid synthesis applications could utilize direct photocrosslinking of hydrogels without inducing any prior thermal crosslinking, and the size of self-assembled spheroids could be controlled by fine-tuning the UV exposure duration. In the cell and hydrogel constructs morphology studies, cell aggregation was observed as early as day 3 in culture, and the spheroids continued to grow and fill the hydrogel matrix over time. These spheroids could be extracted out of the well plates as soon as they have reached the desired size, washed, and further maturated in separate culture plates, before their utilization in variegated applications including tissue biofabrication, disease modeling, and drug discovery. For other applications requiring maintenance of tissue-specific shape, which is highly relevant for multi-layered biofabrication approaches, the matrix properties need to be optimized such that the matrix does not deform over time in culture and the cells are able to attach and proliferate appropriately \$4-56.

As seen in these results, introducing some degree of thermal crosslinking in GelMA matrices prior to photo-crosslinking improves cell elongation (**Figure 5(b)**) and construct fidelity (**Figure 5(c)**). Currently, thermal crosslinking is primarily utilized in extrusion bioprinting approaches

wherein the GelMA bioink is usually allowed to thermally crosslink at lower-than-physiological temperatures in the printhead prior to printing. This imparts the desired viscoelasticity to the bioink and enables shear-thinning to facilitate extrusion through the narrow nozzle while shielding the cells from associated shear forces^{57,58}. However, inducing thermal crosslinking may be challenging with beam scanning and mask projection stereolithography in which, the substrate moves vertically (up or down) through a vat of liquid resin to facilitate layer-wise selective photo-crosslinking of the construct⁵⁹. For two-photon lithography and volumetric bioprinting, however, imparting some degree of thermal crosslinking may be feasible as long as the thermally crosslinked hydrogel is transparent to the incident light^{51,60}.

5. Conclusions

The effects of thermal crosslinking and photo-crosslinking during biofabrication by controlling the pre-photo-crosslinking solution temperature and duration of UV exposure, respectively on the microstructural, mechanical, and biological properties of the GelMA hydrogels were characterized in this work. The results show that enhancing the extent of thermal crosslinking prior to photo-crosslinking increases the matrix entanglement, thereby improving the stiffness and long-term robustness of the hydrogels. Herein, the (80% DOS – 5% w/v) GelMA formulation demonstrated the widest range of stiffness, and constructs fabricated using GelMA solution at low pre-photo-crosslinking temperature (10°C) and moderate UV exposure durations (6, 8 s) allowed the hASC and 3T3 cells to proliferate throughout the matrix, while maintaining the fidelity of the biofabricated constructs. The capability to undergo both thermal and photo-crosslinking expands the applicability of GelMA hydrogels for a variety of biomedical applications. However, it is equally important to understand the nuanced effects of the extent of thermal and photo-crosslinking

on the functionality of the biofabricated tissues, as was demonstrated using the ultrasound-assisted anisotropic tissue biofabrication experiments in this work.

ASSOCIATED CONTENT

Supporting Information

Connecting letters report from Tukey HSD post hoc analysis of compressive stiffness of different hydrogel formulations processed under different thermal- and photo-crosslinking conditions (**Table S1**); ¹H NMR spectra of pure gelatin and GelMA with 40% and 80% DOS (**Figure S1**); Compression moduli of 80% DOS – 5% w/v hydrogels fabricated under different thermal- and photo-crosslinking conditions (**Figure S2**); Graphical representation of the MATLAB algorithm to calculate porosity and pore size of hydrogels and its validation (**Figure S3**)

AUTHOR INFORMATION

Corresponding author

* Rohan A. Shirwaiker, PhD, Associate Professor, Edward P. Fitts Department of Industrial and Systems Engineering, North Carolina State University, Raleigh, NC 27695-7906, USA, email: rashirwaiker@ncsu.edu

Present addresses

^δ Department of Health Sciences & Technology, ETH Zürich, Otto-Stern-Weg 7, 8093 Zürich, Switzerland

Author contributions

R.S. and P.C. conceived the study and developed the experimental framework for the article. P.C. developed the protocols for fabrication and testing of GelMA hydrogels, and performed the experiments related to CryoSEM, cell morphology assessment, and UAB. S.A. performed the experiments related to compression testing and proteolytic degradation. J.C. performed the qPCR experiments and analyses. K.P. performed imaging of the samples in the cell morphology and UAB experiments. R.S. and P.C. contributed equally towards the analyses and inferences, writing the article, and reviewing and refining the manuscript. S.A., J.C., K.P., and J.P. contributed towards the reviewing and refining of the manuscript.

Funding sources

This work is funded by the US National Science Foundation (CMMI #1652489).

ACKNOWLEDGEMENTS

We would like to thank the U.S. National Science Foundation (NSF-CMMI #1652489) for supporting this work. We would also like to thank Dr. Jiaul Hoque (Duke University) for sharing technical insights about GelMA formulations and chemistry.

ABBREVIATIONS

GelMA, Gelatin methacryloyl; CryoSEM, Cryogenic scanning electron microscope/microscopy; UAB, Ultrasound-assisted biofabrication

REFERENCES

- Yue, K.; Trujillo-de Santiago, G.; Alvarez, M. M.; Tamayol, A.; Annabi, N.; Khademhosseini, A. Synthesis, Properties, and Biomedical Applications of Gelatin Methacryloyl (GelMA) Hydrogels. *Biomaterials* 2015, 73, 254–271. https://doi.org/10.1016/J.BIOMATERIALS.2015.08.045.
- (2) Pepelanova, I.; Kruppa, K.; Scheper, T.; Lavrentieva, A. Gelatin-Methacryloyl (GelMA) Hydrogels with Defined Degree of Functionalization as a Versatile Toolkit for 3D Cell Culture and Extrusion Bioprinting. *Bioengineering* **2018**, *5* (3), 55. https://doi.org/10.3390/bioengineering5030055.
- (3) Rizwan, M.; Peh, G. S. L.; Ang, H. P.; Lwin, N. C.; Adnan, K.; Mehta, J. S.; Tan, W. S.; Yim, E. K. F. Sequentially-Crosslinked Bioactive Hydrogels as Nano-Patterned Substrates with Customizable Stiffness and Degradation for Corneal Tissue Engineering Applications. *Biomaterials* 2017, 120, 139–154. https://doi.org/10.1016/j.biomaterials.2016.12.026.
- (4) Serafim, A.; Tucureanu, C.; Petre, D. G.; Dragusin, D. M.; Salageanu, A.; Van Vlierberghe, S.; Dubruel, P.; Stancu, I. C. One-Pot Synthesis of Superabsorbent Hybrid Hydrogels Based on Methacrylamide Gelatin and Polyacrylamide. Effortless Control of Hydrogel Properties through Composition Design. New J. Chem. 2014, 38 (7), 3112–3126. https://doi.org/10.1039/c4nj00161c.
- (5) Chansoria, P.; Etter, E. L.; Nguyen, J. Regenerating Dynamic Organs Using Biomimetic Patches. *Trends Biotechnol.* **2021**. https://doi.org/10.1016/J.TIBTECH.2021.07.001.
- (6) Zhao, X.; Sun, X.; Yildirimer, L.; Lang, Q.; Zhang, Y.; Cui, W.; Annabi, N.; Khademhosseini, A.; Arabia, S.; Surgery, R. HHS Public Access. **2018**, 66–77.

- https://doi.org/10.1016/j.actbio.2016.11.017.Cell.
- (7) Davey, S. K.; Aung, A.; Agrawal, G.; Lim, H. L.; Kar, M.; Varghese, S. Embedded 3D Photopatterning of Hydrogels with Diverse and Complex Architectures for Tissue Engineering and Disease Models. *Tissue Eng. Part C Methods* **2015**, *21* (11), 1188–1196. https://doi.org/10.1089/ten.tec.2015.0179.
- (8) Chansoria, P.; Shirwaiker, R. 3D Bioprinting of Anisotropic Engineered Tissue Constructs with Ultrasonically Induced Cell Patterning. *Addit. Manuf.* 2020, 32, 101042. https://doi.org/10.1016/j.addma.2020.101042.
- (9) Yung, C. W.; Wu, L. Q.; Tullman, J. A.; Payne, G. F.; Bentley, W. E.; Barbari, T. A. Transglutaminase Crosslinked Gelatin as a Tissue Engineering Scaffold. *J. Biomed. Mater. Res. Part A* 2007, 83A (4), 1039–1046. https://doi.org/10.1002/jbm.a.31431.
- (10) Lee, B. H.; Lum, N.; Seow, L. Y.; Lim, P. Q.; Tan, L. P. Synthesis and Characterization of Types A and B Gelatin Methacryloyl for Bioink Applications. *Materials (Basel)*. 2016, 9
 (10), 797. https://doi.org/10.3390/ma9100797.
- (11) Pahoff, S.; Meinert, C.; Bas, O.; Nguyen, L.; Klein, T. J.; Hutmacher, D. W. Effect of Gelatin Source and Photoinitiator Type on Chondrocyte Redifferentiation in Gelatin Methacryloyl-Based Tissue-Engineered Cartilage Constructs. *J. Mater. Chem. B* 2019, 7 (10), 1761–1772. https://doi.org/10.1039/c8tb02607f.
- (12) Monteiro, N.; Thrivikraman, G.; Athirasala, A.; Tahayeri, A.; França, C. M.; Ferracane, J. L.; Bertassoni, L. E. Photopolymerization of Cell-Laden Gelatin Methacryloyl Hydrogels Using a Dental Curing Light for Regenerative Dentistry. *Dent. Mater.* 2018, 34 (3), 389–399. https://doi.org/10.1016/j.dental.2017.11.020.
- (13) Billiet, T.; Gevaert, E.; De Schryver, T.; Cornelissen, M.; Dubruel, P. The 3D Printing of

- Gelatin Methacrylamide Cell-Laden Tissue-Engineered Constructs with High Cell Viability. *Biomaterials* **2014**, *35* (1), 49–62. https://doi.org/10.1016/j.biomaterials.2013.09.078.
- (14) Ying, G.; Jiang, N.; Yu, C.; Zhang, Y. S. Three-Dimensional Bioprinting of Gelatin Methacryloyl (GelMA). *Bio-Design and Manufacturing*. Springer December 1, 2018, pp 215–224. https://doi.org/10.1007/s42242-018-0028-8.
- (15) Tigner, T. J.; Rajput, S.; Gaharwar, A. K.; Alge, D. L. Comparison of Photo Cross Linkable Gelatin Derivatives and Initiators for Three-Dimensional Extrusion Bioprinting. *Biomacromolecules* 2020, 21 (2), 454–463. https://doi.org/10.1021/acs.biomac.9b01204.
- (16) Chansoria, P.; Schuchard, K.; Shirwaiker, R. A. Process Hybridization Schemes for Multiscale Engineered Tissue Biofabrication. WIREs Nanomedicine and Nanobiotechnology 2020. https://doi.org/10.1002/wnan.1673.
- (17) Salem, A. K.; Stevens, R.; Pearson, R. G.; Davies, M. C.; Tendler, S. J. B.; Roberts, C. J.; Williams, P. M.; Shakesheff, K. M. Interactions of 3T3 Fibroblasts and Endothelial Cells with Defined Pore Features. *J. Biomed. Mater. Res.* 2002, 61 (2), 212–217. https://doi.org/10.1002/jbm.10195.
- (18) Chan, V.; Zorlutuna, P.; Jeong, J. H.; Kong, H.; Bashir, R. Three-Dimensional Photopatterning of Hydrogels Using Stereolithography for Long-Term Cell Encapsulation. *Lab Chip* **2010**, *10* (16), 2062. https://doi.org/10.1039/c004285d.
- (19) Wang, Z.; Abdulla, R.; Parker, B.; Samanipour, R.; Ghosh, S.; Kim, K. A Simple and High-Resolution Stereolithography-Based 3D Bioprinting System Using Visible Light Crosslinkable Bioinks. *Biofabrication* 2015, 7 (4), 045009. https://doi.org/10.1088/1758-5090/7/4/045009.

- (20) Narayanan, L. K.; Huebner, P.; Fisher, M. B.; Spang, J. T.; Starly, B.; Shirwaiker, R. A.; Fitts, E. P. 3D-Bioprinting of Polylactic Acid (PLA) Nanofiber—Alginate Hydrogel Bioink Containing Human Adipose-Derived Stem Cells. *ACS Biomater. Sci. Eng.* **2016**, *2* (10), 1732–1742. https://doi.org/10.1021/acsbiomaterials.6b00196.
- (21) Kim, C.; Young, J. L.; Holle, A. W.; Jeong, K.; Major, L. G.; Jeong, J. H.; Aman, Z. M.; Han, D. W.; Hwang, Y.; Spatz, J. P.; Choi, Y. S. Stem Cell Mechanosensation on Gelatin Methacryloyl (GelMA) Stiffness Gradient Hydrogels. *Ann. Biomed. Eng.* 2020, 48 (2), 893–902. https://doi.org/10.1007/s10439-019-02428-5.
- (22) Hamid, A. A.; Idrus, R. B. H.; Saim, A. Bin; Sathappan, S.; Chua, K. H. Characterization of Human Adipose-Derived Stem Cells and Expression of Chondrogenic Genes during Induction of Cartilage Differentiation. *Clinics* 2012, 67 (2), 99–106. https://doi.org/10.6061/clinics/2012(02)03.
- (23) Brake, D. K.; Smith, E. O. B.; Mersmann, H.; Smith, C. W.; Robker, R. L. ICAM-1 Expression in Adipose Tissue: Effects of Diet-Induced Obesity in Mice. *Am. J. Physiol. Cell Physiol.* **2006**, *291* (6), 1232–1239. https://doi.org/10.1152/ajpcell.00008.2006.
- (24) Wei, L.; Yin, F.; Zhang, W.; Li, L. ITGA 1 and Cell Adhesion-Mediated Drug Resistance in Ovarian Cancer. **2017**.
- Wang, H.; Jin, P.; Sabatino, M.; Ren, J.; Civini, S.; Bogin, V.; Ichim, T. E.; Stroncek, D.
 F. Comparison of Endometrial Regenerative Cells and Bone Marrow Stromal Cells. *J. Transl. Med.* 2012, *10* (1), 1–14. https://doi.org/10.1186/1479-5876-10-207.
- (26) Chansoria, P.; Narayanan, L. K.; Schuchard, K.; Shirwaiker, R. A. Ultrasound-Assisted Biofabrication and Bioprinting of Preferentially Aligned Three-Dimensional Cellular Constructs. *Biofabrication* 2019, 11 (3), 14861. https://doi.org/10.1088/1758-5090/ab15cf.

- (27) Chansoria, P.; Shirwaiker, R. Characterizing the Process Physics of Ultrasound-Assisted Bioprinting. *Sci. Rep.* **2019**, *9* (1), 13889. https://doi.org/10.1038/s41598-019-50449-w.
- (28) Xu, H.; Casillas, J.; Krishnamoorthy, S.; Xu, C. Effects of Irgacure 2959 and Lithium Phenyl-2,4,6-Trimethylbenzoylphosphinate on Cell Viability, Physical Properties, and Microstructure in 3D Bioprinting of Vascular-like Constructs. *Biomed. Mater.* **2020**, *15* (5), 055021. https://doi.org/10.1088/1748-605X/ab954e.
- (29) Holmes, R.; Yang, X.-B.; Dunne, A.; Florea, L.; Wood, D.; Tronci, G. Thiol-Ene Photo-Click Collagen-PEG Hydrogels: Impact of Water-Soluble Photoinitiators on Cell Viability, Gelation Kinetics and Rheological Properties. *Polym. 2017, Vol. 9, Page 226* 2017, 9 (6), 226. https://doi.org/10.3390/POLYM9060226.
- (30) Costantini, M.; Testa, S.; Fornetti, E.; Barbetta, A.; Trombetta, M.; Cannata, S. M.; Gargioli, C.; Rainer, A. Engineering Muscle Networks in 3d Gelatin Methacryloyl Hydrogels: Influence of Mechanical Stiffness and Geometrical Confinement. *Front. Bioeng. Biotechnol.* 2017, 5 (APR), 22. https://doi.org/10.3389/fbioe.2017.00022.
- (31) Tomlins, P.; Grant, P. V; Mikhalovsky, S.; Mikhalovska, L.; James, S.; Vadgama, P. Characterisation of Polymeric Tissue Scaffolds; 2006; Vol. 89.
- (32) Ouyang, L. Biological Characterization and Applications. In *Study on Microextrusion-based 3D Bioprinting and Bioink Crosslinking Mechanisms*; Springer, Singapore, 2019; pp 105–125. https://doi.org/10.1007/978-981-13-9455-3_7.
- (33) Schindelin, J.; Arganda-Carreras, I.; Frise, E.; Kaynig, V.; Longair, M.; Pietzsch, T.; Preibisch, S.; Rueden, C.; Saalfeld, S.; Schmid, B.; Tinevez, J.-Y.; White, D. J.; Hartenstein, V.; Eliceiri, K.; Tomancak, P.; Cardona, A. Fiji: An Open-Source Platform for Biological-Image Analysis. *Nat. Methods* **2012**, *9* (7), 676–682.

- https://doi.org/10.1038/nmeth.2019.
- (34) Armstrong, J. P. K.; Puetzer, J. L.; Serio, A.; Guex, A. G.; Kapnisi, M.; Breant, A.; Zong, Y.; Assal, V.; Skaalure, S. C.; King, O.; Murty, T.; Meinert, C.; Franklin, A. C.; Bassindale, P. G.; Nichols, M. K.; Terracciano, C. M.; Hutmacher, D. W.; Drinkwater, B. W.; Klein, T. J.; Perriman, A. W.; Stevens, M. M. Engineering Anisotropic Muscle Tissue Using Acoustic Cell Patterning. *Adv. Mater.* 2018, 30 (43). https://doi.org/10.1002/adma.201802649.
- (35) Barber, R. D.; Harmer, D. W.; Coleman, R. A.; Clark, B. J. GAPDH as a Housekeeping Gene: Analysis of GAPDH MRNA Expression in a Panel of 72 Human Tissues. *Physiol. Genomics* **2005**, *21* (3), 389–395. https://doi.org/10.1152/physiolgenomics.00025.2005.
- (36) Li, J.; Mooney, D. J. Designing Hydrogels for Controlled Drug Delivery. *Nature Reviews Materials*. Nature Publishing Group October 18, 2016, pp 1–17. https://doi.org/10.1038/natrevmats.2016.71.
- (37) Sun, M.; Chi, G.; Li, P.; Lv, S.; Xu, J.; Xu, Z.; Xia, Y.; Tan, Y.; Xu, J.; Li, L.; Li, Y. Effects of Matrix Stiffness on the Morphology, Adhesion, Proliferation and Osteogenic Differentiation of Mesenchymal Stem Cells. *Int. J. Med. Sci.* **2018**, *15* (3), 257–268. https://doi.org/10.7150/ijms.21620.
- (38) Li, X.; Chen, S.; Li, J.; Wang, X.; Zhang, J.; Kawazoe, N.; Chen, G. 3D Culture of Chondrocytes in Gelatin Hydrogels with Different Stiffness. *Polymers (Basel)*. 2016, 8 (8), 269. https://doi.org/10.3390/polym8080269.
- (39) Mildmay-White, A.; Khan, W. Cell Surface Markers on Adipose-Derived Stem Cells: A Systematic Review1. Mildmay-White A, Khan W. Cell Surface Markers on Adipose-Derived Stem Cells: A Systematic Review. Curr Stem Cell Res Ther. 2017;12(6):484-492.

- Doi:10.2174/1574888X11666160429122133. Curr. Stem Cell Res. Ther. **2017**, 12 (6), 484–492. https://doi.org/10.2174/1574888X11666160429122133.
- (40) Taechangam, N.; Iyer, S. S.; Walker, N. J.; Arzi, B.; Borjesson, D. L. Mechanisms Utilized by Feline Adipose-Derived Mesenchymal Stem Cells to Inhibit T Lymphocyte Proliferation. *Stem Cell Res. Ther.* **2019**, *10* (1), 1–12. https://doi.org/10.1186/s13287-019-1300-3.
- (41) Echave, M. C.; Burgo, L. S.; Pedraz, J. L.; Orive, G. Gelatin as Biomaterial for Tissue Engineering. *Curr. Pharm. Des.* 2017, 23 (24).
 https://doi.org/10.2174/0929867324666170511123101.
- (42) Lee, K. Y.; Mooney, D. J. Alginate: Properties and Biomedical Applications. *Prog. Polym. Sci.* 2012, 37 (1), 106–126. https://doi.org/10.1016/J.PROGPOLYMSCI.2011.06.003.
- (43) Bengestrate, L.; Virtue, S.; Campbell, M.; Vidal-Puig, A.; Hadaschik, D.; Hahn, P.; Bielke, W. Genome-Wide Profiling of MicroRNAs in Adipose Mesenchymal Stem Cell Differentiation and Mouse Models of Obesity. *PLoS One* **2011**, *6* (6), e21305. https://doi.org/10.1371/journal.pone.0021305.
- (44) Zohora, F. T.; Aldebs, A. I.; Nosoudi, N.; Singh, S. P.; Ramirez-Vick, J. E. Gene Expression Profiling of Human Adipose Tissue Stem Cells during 2D versus 3D Adipogenesis. *Cells Tissues Organs* 2019, 208 (3–4), 113–133. https://doi.org/10.1159/000507187.
- (45) Su, Y.; Denbeigh, J. M.; Camilleri, E. T.; Riester, S. M.; Parry, J. A.; Wagner, E. R.; Yaszemski, M. J.; Dietz, A. B.; Cool, S. M.; van Wijnen, A. J.; Kakar, S. Extracellular Matrix Protein Production in Human Adipose-Derived Mesenchymal Stem Cells on

- Three-Dimensional Polycaprolactone (PCL) Scaffolds Responds to GDF5 or FGF2. *Gene Reports* **2018**, *10*, 149–156. https://doi.org/10.1016/j.genrep.2017.12.004.
- (46) Jung, Y. J.; Kim, H. K.; Cho, Y.; Choi, J. S.; Woo, C. H.; Lee, K. S.; Sul, J. H.; Lee, C. M.; Han, J.; Park, J. H.; Jo, D. G.; Cho, Y. W. Cell Reprogramming Using Extracellular Vesicles from Differentiating Stem Cells into White/Beige Adipocytes. *Sci. Adv.* 2020, 6 (13), eaay6721. https://doi.org/10.1126/sciadv.aay6721.
- (47) Liu, X.; Xiang, Q.; Xu, F.; Huang, J.; Yu, N.; Zhang, Q.; Long, X.; Zhou, Z. Single-Cell RNA-Seq of Cultured Human Adipose-Derived Mesenchymal Stem Cells. *Sci. Data* **2019**, 6 (1), 1–8. https://doi.org/10.1038/sdata.2019.31.
- (48) Guimarães, C. F.; Gasperini, L.; Marques, A. P.; Reis, R. L. The Stiffness of Living Tissues and Its Implications for Tissue Engineering. *Nature Reviews Materials*. Nature Research February 21, 2020, pp 1–20. https://doi.org/10.1038/s41578-019-0169-1.
- (49) O'Connell, C. D.; Zhang, B.; Onofrillo, C.; Duchi, S.; Blanchard, R.; Quigley, A.; Bourke, J.; Gambhir, S.; Kapsa, R.; Di Bella, C.; Choong, P.; Wallace, G. G. Tailoring the Mechanical Properties of Gelatin Methacryloyl Hydrogels through Manipulation of the Photocrosslinking Conditions. *Soft Matter* 2018, 14 (11), 2142–2151. https://doi.org/10.1039/c7sm02187a.
- (50) Bernal, P. N.; Delrot, P.; Loterie, D.; Li, Y.; Malda, J.; Moser, C.; Levato, R. Volumetric Bioprinting of Complex Living-Tissue Constructs within Seconds. *Adv. Mater.* **2019**, *31* (42), 1904209. https://doi.org/10.1002/adma.201904209.
- (51) Loterie, D.; Delrot, P.; Moser, C. High-Resolution Tomographic Volumetric Additive Manufacturing. *Nat. Commun.* **2020**, *11* (1), 852. https://doi.org/10.1038/s41467-020-14630-4.

- Vunjak-Novakovic, G.; Tandon, N.; Godier, A.; Maidhof, R.; Marsano, A.; Martens, T.
 P.; Radisic, M. Challenges in Cardiac Tissue Engineering. *Tissue engineering. Part B, Reviews*. Mary Ann Liebert, Inc. 140 Huguenot Street, 3rd Floor New Rochelle, NY
 10801 USA October 13, 2010, pp 169–187. https://doi.org/10.1089/ten.teb.2009.0352.
- (53) Wang, T.; Gardiner, B. S.; Lin, Z.; Rubenson, J.; Kirk, T. B.; Wang, A.; Xu, J.; Smith, D. W.; Lloyd, D. G.; Zheng, M. H. Bioreactor Design for Tendon/Ligament Engineering. *Tissue Engineering Part B: Reviews*. Mary Ann Liebert, Inc. April 1, 2013, pp 133–146. https://doi.org/10.1089/ten.teb.2012.0295.
- (54) Lou, Y. R.; Leung, A. W. Next Generation Organoids for Biomedical Research and Applications. *Biotechnology Advances*. Elsevier Inc. January 1, 2018, pp 132–149. https://doi.org/10.1016/j.biotechadv.2017.10.005.
- (55) Bajaj, P.; Schweller, R. M.; Khademhosseini, A.; West, J. L.; Bashir, R. 3D Biofabrication Strategies for Tissue Engineering and Regenerative Medicine. *Annu. Rev. Biomed. Eng.*2014, 16 (1), 247–276. https://doi.org/10.1146/annurev-bioeng-071813-105155.
- (56) Melchels, F. P. W.; Domingos, M. A. N.; Klein, T. J.; Malda, J.; Bartolo, P. J.; Hutmacher, D. W. Additive Manufacturing of Tissues and Organs. *Progress in Polymer Science*. Elsevier Ltd August 1, 2012, pp 1079–1104. https://doi.org/10.1016/j.progpolymsci.2011.11.007.
- (57) Starly, B.; Shirwaiker, R. A. Three-Dimensional Bioprinting. In 3D Bioprinting and Nanotechnology in Tissue Engineering and Regenerative Medicine; Zhang, L., Fisher, J. P., Leong, K., Eds.; Academic Press: Waltham, 2015; pp 57–77.
- (58) Dababneh, A. B.; Ozbolat, I. T. Bioprinting Technology: A Current State-of-the-Art Review. *J. Manuf. Sci. Eng.* **2014**, *136* (6), 061016. https://doi.org/10.1115/1.4028512.

- (59) Cui, H.; Nowicki, M.; Fisher, J. P.; Zhang, L. G. 3D Bioprinting for Organ Regeneration. *Adv. Healthc. Mater.* **2017**, *6* (1), 1601118. https://doi.org/10.1002/adhm.201601118.
- (60) Nguyen, A. K.; Narayan, R. J. Two-Photon Polymerization for Biological Applications.
 Materials Today. Elsevier B.V. July 1, 2017, pp 314–322.
 https://doi.org/10.1016/j.mattod.2017.06.004.

For Table of Contents Use Only

Parth Chansoria, PhD ^{1,2, \delta}, Suleman Asif ^{1,2}, Kathryn Polkoff ^{2,3}, Jaewook Chung, PhD ^{2,3}, Jorge A. Piedrahita, PhD ^{2,3}, Rohan A. Shirwaiker, PhD^{1,2,4,5*}

